AIAA JOURNAL
Vol. 41, No. 9, September 2003

Dynamic Analysis of Composite Laminates with Multiple Delamination Using Improved Layerwise Theory

Heung Soo Kim,* Aditi Chattopadhyay,† and Anindya Ghoshal‡
Arizona State University, Tempe, Arizona 85287-6106

A procedure has been developed to investigate the dynamic response of composite structures, with embedded multiple delaminations. A recently developed improved layerwise composite laminate theory is extended to model composite laminates of moderately large thickness with delamination. The theory accurately predicts interlaminar shear stresses while maintaining computational efficiency. Natural frequencies and mode shapes are computed for cross-ply laminates with delaminations placed at different locations. Experiments are conducted to validate the developed theory. Numerical results indicate excellent correlation with analytical solutions and experimental results. Parametric studies are conducted to investigate the effect of delamination location, both through the thickness and in plane, and number of delaminations on the dynamic response. A potential application of the developed procedure is in structural health monitoring where accurate predictions of dynamic response in the presence of delamination are important issues.

I. Introduction

A SIGNIFICANT amount of research has been performed on modeling composite laminates in the presence of delamination.[1–14] In the analysis of composite laminates, classical laminate theory (CLT) and first-order shear deformation theory (FSDT) have been conventionally used to model laminated structures. It is well known that CLT ignores transverse shear stresses and FSDT does not provide sufficient accuracy because of the use of shear correction factors. The layerwise approach introduced by Barbero and Reddy[1] is an alternative because it is capable of modeling displacement discontinuities. However, computational effort increases with the number of plies. A refined higher-order theory has been developed by Chattopadhyay and Gu to model the presence of delamination in composite plates and shells of moderately thick constructions.[2,3] Their theory was shown to agree well with both elasticity solutions[4] and experimental results.[5] However, although the higher-order-basedtheories provide good accuracy at the global level, they fail to satisfy stress continuity at ply interfaces. Recently, Zhou and Chattopadhyay[6] reported the development of a new layerwise shell theory addressing some of these issues. However, their work did not include the presence of delaminations. To investigate the dynamic characteristics of composites with delaminations, Shen and Grady[7] studied the free vibration of delaminated composite beam using Timoshenko beam theory. Crawley and Adams[8] and Williams et al.[9] investigated the shift in natural frequencies caused by damage. However, the highly anisotropic characteristics of laminated composites leads to only minor changes in the natural frequencies and displacement mode shapes for relatively large delaminations. Less than 2–3% changes in the fundamental frequency were reported, in the literature, with delamination area as large as 20% (of the composite structure). Luo and Hanagud[10] proposed two delamination coefficients to discern the delamination modes and discussed the possibility of detecting delamination size and location based on the modal analysis results. A study on the dynamic response of delaminated beams had been performed by Lestari and Hanagud.[11] Thornburgh and Chattopadhyay[12] developed a unified approach to model the presence of two types of damage, delaminations and transverse matrix cracks in composites. They further extended their model to study the effect of delamination on the dynamic response of smart composite structures.[13] Cho and Kim[14,15] developed a higher-order zig-zag theory for laminated composite plates with multiple delaminations. Recently, Kim et al.[16] developed an improved layerwise theory to investigate interlaminar stresses in smart composite structures. In the present paper this new layerwise theory is further extended for modeling composite laminated plates with embedded multiple delamination ensuring global and local ply level accuracy.

Received 24 July 2002; revision received 19 February 2003; accepted for publication 24 February 2003.

*Graduate Research Associate, Department of Mechanical and Aerospace Engineering. Student Member AIAA.

†Professor, Department of Mechanical and Aerospace Engineering; aditi@asu.edu. Associate Fellow AIAA.

‡Research Professor, Department of Mechanical and Aerospace Engineering; currently National Research Council Associate, Nondestructive Evaluation Sciences Branch, NASA Langley Research Center, MS 231, 3B East Taylor Street, Building 1230B/Room 190, Hampton, VA 23681-2199. Senior Member AIAA.

II. Mathematical Theory

Accurate description of structural deformation is a key issue in modeling composites of arbitrary thickness. In the presence of delamination, interlaminar stresses also play a critical role. Therefore, the filed description must be capable of accurate estimation of these stresses. The improved layerwise theory developed by Kim et al.[16] is used to address this issue. In this theory the first-order shear deformation based displacement field is used to address the overall response of the entire laminate, and layerwise functions are used to accommodate the complexity of zig-zag-like in-plane deformation through the laminate thickness, while satisfying interlaminar shear traction continuity conditions. This theory is now extended to include the presence of multiple delaminations.

To model delamination, the assumed displacement field is supplemented with Heaviside unit step functions, which allows introduction of independent displacement field above and below the sublaminates. Consider a N-layered laminated composite plate with multiple delaminations. The displacements of a point with coordinates (x, y, z) are described using the superposition of first-order shear deformation and layerwise functions, as follows:

$$U_i^k(x, y, z, t) = u_i(x, y, t) + \phi_i(x, y, t)z + \theta_i^k(x, y, t)g(z) + \psi_i^k(x, y, t)h(z) + \sum_{j=1}^{N-1} \bar{u}_i^j(x, y, t)H(z - z_j)$$

$$U_3^k(x, y, z, t) = w(x, y, t) + \sum_{j=1}^{N-1} \bar{w}^j(x, y, t)H(z - z_j) \qquad (1)$$

where U_i^k denotes in-plane displacement and U_3^k denotes transverse deflection. The subscript i denotes the coordinate x or y and the

superscript k denotes the kth layer of the laminate. The quantities u_i and w denote the displacement of the reference plane, ϕ_i are rotations of the normal to the reference plane about the x and y axes, and quantities θ_i^k and ψ_i^k are layerwise structural unknowns defined at each lamina. The terms $\bar{u}_i^j$ and $\bar{w}^j$ represent possible jumps in displacement field caused by delamination allowing slipping and separation between sublaminates, and z_j denotes the delaminated interface. The function $H(z - z_j)$ is a Heaviside unit step function. All interfaces between layers are initially assumed to be delaminated. Then, the number of delaminated layer interfaces is equal to the total number of ply interfaces. Perfectly bonded interfaces can be easily simulated by setting $\bar{u}_i^j$ and $\bar{w}^j$ to be zero at these interfaces. The through-laminate-thickness functions $g(z)$ and $h(z)$ are used to address the characteristics of in-plane zig-zag deformation and have the following form:

$$g(z) = \sinh(z/h), \qquad h(z) = \cosh(z/h) \tag{2}$$

where functions $g(z)$ and $h(z)$ render higher-order odd and even distributions, respectively.

In the preceding formulation the unknowns are u_i, ϕ_i, w, θ_i^k, ψ_i^k, $\bar{u}_i^j$, and $\bar{w}^j$ leading to a total of $5 + 4N + 3(N-1)$ structural unknowns for a N-layered laminate. Thus, the total number of structural unknowns is dependent on the number of layers and delaminations, implying that computational effort will increase greatly if multilayered laminates are used. A reduction in the number of structural variables is essential for the model to be computationally efficient and useful in practical applications. Therefore, a procedure is developed to reduce the number of variables by enforcing continuity of the transverse shear stresses and the in-plane displacement at ply interfaces, as described next.

The displacement field described in Eq. (1) does not satisfy the requirement of shear traction-free boundary conditions at free surfaces. It also does not ensure continuity of transverse stresses and in-plane displacement at ply interfaces. The surface traction-free boundary conditions on the top and bottom surfaces are imposed as follows:

$$\tau_{iz}^1(x, y, z_1) = 0, \qquad \tau_{iz}^N(x, y, z_{N+1}) = 0 \tag{3}$$

where τ_{iz} denotes transverse shear stress and the quantities z_1 and z_{N+1} denote the thickness coordinates of the bottom and the top surfaces, respectively. For orthotropic laminate the transverse shear stresses depend on transverse shear strains. Thus, the traction-free condition can be rewritten as follows:

$$\phi_i + g_{,z}\psi_i^1 + h_{,z}\theta_i^1 + w_{,i} = 0 \qquad \text{at} \qquad z = z_1$$

$$\phi_i + g_{,z}\psi_i^N + h_{,z}\theta_i^N + w_{,i} + \sum_{j=1}^{N-1} \bar{w}_{,i}^j H(z - z_j) = 0 \qquad \text{at} \qquad z = z_{N+1} \tag{4}$$

where $(\,)_{,i}$ and $(\,)_{,z}$ denote partial derivatives with respect to x, y, and z coordinates, respectively.

The transverse shear-stress continuity conditions can be written as follows:

$$\tau_{iz}^k(x, y, z_{k+1}) = \tau_{iz}^{k+1}(x, y, z_{k+1}) \tag{5}$$

The condition of zero shear stresses at delaminated interfaces are mathematically satisfied by the preceding equation. Using Hooke's law and kinematic relations, these conditions can be expressed as follows:

$$Q_{55}^{(k)}\left[\phi_1 + g_{,z}(z_{k+1})\theta_1^k + h_{,z}(z_{k+1})\psi_1^k + w_{,x} + \sum_{j=1}^{k} \bar{w}_{,x}^j H(z - z_j)\right]$$

$$= Q_{55}^{(k+1)}\left[\phi_1 + g_{,z}(z_{k+1})\theta_1^{k+1} + h_{,z}(z_{k+1})\psi_1^{k+1} + w_{,x} + \sum_{j=1}^{k+1} \bar{w}_{,x}^j H(z - z_j)\right]$$

$$Q_{44}^{(k)}\left[\phi_2 + g_{,z}(z_{k+1})\theta_2^k + h_{,z}(z_{k+1})\psi_2^k + w_{,y} + \sum_{j=1}^{k} \bar{w}_{,y}^j H(z - z_j)\right]$$

$$= Q_{44}^{(k+1)}\left[\phi_2 + g_{,z}(z_{k+1})\theta_2^{k+1} + h_{,z}(z_{k+1})\psi_2^{k+1} + w_{,y} + \sum_{j=1}^{k+1} \bar{w}_{,y}^j H(z - z_j)\right] \tag{6}$$

where $Q_{44}^{(k)}$ and $Q_{55}^{(k)}$ are the reduced stiffness of the kth lamina.

Furthermore, at the perfectly bonded interfaces the in-plane displacements are continuous at each interface. The displacements are also assumed to be continuous at the delaminated interface, allowing slipping effect. The continuity conditions of in-plane displacements, at the kth interface, can be expressed as follows:

$$g(z_{k+1})\theta_i^k + h(z_{k+1})\psi_i^k = g(z_{k+1})\theta_i^{k+1} + h(z_{k+1})\psi_i^{k+1} \tag{7}$$

By using Eqs. (4), (6), and (7), the structural unknowns of the kth layer are related to those of the $(k-1)$th layer. Thus, for a N-layer laminated composite with multiple delaminations, $4N$ constraint conditions are obtained. By substituting the $4N$ equations into the assumed displacement field [Eq. (1)], the in-plane displacements of the cross-ply laminate are expressed as follows:

$$U_1^k(x, y, z, t) = u_1 + A_1^k(z)\phi_1 + B_1^k(z)w_{,x} + \bar{C}_1^j(z)\bar{w}_{,x}^j + \sum_{j=1}^{N-1} \bar{u}_1^j H(z - z_j)$$

$$U_2^k(x, y, z, t) = u_2 + A_2^k(z)\phi_2 + B_2^k(z)w_{,y} + \bar{C}_2^j(z)\bar{w}_{,y}^j + \sum_{j=1}^{N-1} \bar{u}_2^j H(z - z_j) \tag{8}$$

where

$$A_1^k(z) = z + a_1^k g(z) + c_1^k h(z), \qquad A_2^k(z) = z + a_2^k g(z) + c_2^k h(z)$$

$$B_1^k(z) = a_1^k g(z) + c_1^k h(z), \qquad B_2^k(z) = a_2^k g(z) + c_2^k h(z)$$

$$\bar{C}_1^j(z) = \bar{b}_1^j g(z) + \bar{d}_1^j h(z), \qquad \bar{C}_2^j(z) = \bar{b}_2^j g(z) + \bar{d}_2^j h(z) \tag{9}$$

The layerwise coefficients a_1^k, a_2^k, c_1^k, c_2^k, $\bar{b}_1^j$, $\bar{b}_2^j$, $\bar{d}_1^j$, and $\bar{d}_2^j$ are obtained from the $4N$ constraint equations and are expressed in term of laminate geometry and material properties. The coefficients a_1^k, a_2^k, c_1^k, and c_2^k represent scalar quantities at each layer. However, coefficients $\bar{b}_1^j$, $\bar{b}_2^j$, $\bar{d}_1^j$, and $\bar{d}_2^j$ are $1 \times (N-1)$ row vectors at each layer and describe the opening effect caused by delamination at each interface. Therefore, the displacement field, ranging from the first layer to the Nth layer, can be expressed in terms of the variables u_1, u_2, w, ϕ_1, ϕ_2, $\bar{u}_1^j$, $\bar{u}_2^j$, and $\bar{w}^j$, making it dependent on the number of delamination but independent of the number of layers.

III. Finite Element Implementation

The preceding formulation is implemented using the finite element method. The primary displacement unknowns are expressed in terms of nodal values and shape functions as follows:

$$\left(u_1, u_2, \phi_1, \phi_2, \bar{u}_1^j, \bar{u}_2^j\right) = \sum_{m=1}^{n} N_m\left[(u_1)_m, (u_2)_m, (\phi_1)_m, (\phi_2)_m, \left(\bar{u}_1^j\right)_m, \left(\bar{u}_2^j\right)_m\right]$$

$$w = \sum_{m=1}^{n} [H_m(w)_m + H_{xm}(w_{,x})_m + H_{ym}(w_{,y})_m]$$

$$\bar{w}^j = \sum_{m=1}^{n} [H_m(\bar{w})_m + H_{xm}(\bar{w}_{,x})_m + H_{ym}(\bar{w}_{,y})_m] \tag{10}$$

where n is the number of nodes in an element; N_m is a Lagrange interpolation function; and H_m, H_{xm}, and H_{ym} are Hermite interpolation functions. In this paper four-noded plate element is used with linear Lagrange interpolation functions to describe the in-plane unknowns, and Hermite cubic interpolation functions are used for the out-of-plane unknowns.

ciated strain field $\varepsilon(x, y, z, t)$ can be written as follows:

$$\boldsymbol{u}(x, y, z, t) = \boldsymbol{L}_u \boldsymbol{u}^e(x, y, t), \qquad \varepsilon(x, y, z, t) = \boldsymbol{L}_\varepsilon \boldsymbol{u}^e(x, y, t) \tag{14}$$

where the higher-order operators L_u and L_ε are defined as follows:

$$\boldsymbol{L}_u = \begin{bmatrix} 1 & 0 & B_1^k(z)\dfrac{\partial}{\partial x} & A_1^k(z) & 0 & \bar{H}^D & \bar{0}^D & \bar{C}_1^j(z)\dfrac{\partial}{\partial x} \\ 0 & 1 & B_2^k(z)\dfrac{\partial}{\partial y} & 0 & A_2^k(z) & \bar{0}^D & \bar{H}^D & \bar{C}_2^j(z)\dfrac{\partial}{\partial y} \\ 0 & 0 & 1 & 0 & 0 & \bar{0}^D & \bar{0}^D & \bar{H}^D \end{bmatrix} \tag{15}$$

$$\boldsymbol{L}_\varepsilon = \begin{bmatrix} \dfrac{\partial}{\partial x} & 0 & B_1^k(z)\dfrac{\partial^2}{\partial x^2} & A_1^k(z)\dfrac{\partial}{\partial x} & 0 & \bar{H}^D\dfrac{\partial}{\partial x} & \bar{0}^D & \bar{C}_1^j(z)\dfrac{\partial^2}{\partial x^2} \\ 0 & \dfrac{\partial}{\partial y} & B_2^k(z)\dfrac{\partial^2}{\partial y^2} & 0 & A_2^k(z)\dfrac{\partial}{\partial y} & \bar{0}^D & \bar{H}^D\dfrac{\partial}{\partial y} & \bar{C}_2^j(z)\dfrac{\partial^2}{\partial y^2} \\ 0 & 0 & \left[1 + B_{2,z}^k(z)\right]\dfrac{\partial}{\partial y} & 0 & A_{2,z}^k(z) & \bar{0}^D & \bar{0}^D & \left[\bar{C}_{2,z}^j(z) + \bar{H}^D\right]\dfrac{\partial}{\partial y} \\ 0 & 0 & \left[1 + B_{1,z}^k(z)\right]\dfrac{\partial}{\partial x} & A_{1,z}^k(z) & 0 & \bar{0}^D & \bar{0}^D & \left[\bar{C}_{1,z}^j(z) + \bar{H}^D\right]\dfrac{\partial}{\partial x} \\ \dfrac{\partial}{\partial y} & \dfrac{\partial}{\partial x} & \left[B_1^k(z) + B_2^k(z)\right]\dfrac{\partial^2}{\partial x \partial y} & A_1^k(z)\dfrac{\partial}{\partial y} & A_2^k(z)\dfrac{\partial}{\partial x} & \bar{H}^D\dfrac{\partial}{\partial y} & \bar{H}^D\dfrac{\partial}{\partial x} & \left[\bar{C}_1^j(z) + \bar{C}_2^j(z)\right]\dfrac{\partial^2}{\partial x \partial y} \end{bmatrix}$$

$$\bar{H}^D = [H(z - z_1) \quad \cdots \quad H(z - z_j)]$$

The relationship between displacement unknowns and nodal unknowns in Eq. (10) can be expressed by the following matrix form:

$$\{u^e\} = [N]\{d\} \tag{11}$$

where

$$\{u^e\} = \left[u_1, u_2, w, \phi_1, \phi_2, \bar{u}_1^j, \bar{u}_2^j, \bar{w}^j\right]^T$$

$$\{d\} = \left[\ldots, u_{1i}, u_{2i}, w_i, w_{,xi}, w_{,yi}, \phi_{1i}, \phi_{2i}, \bar{u}_{1i}^j, \bar{u}_{2i}^j, \bar{w}_{,i}^j, \bar{w}_{,xi}^j, \bar{w}_{,yi}^j, \ldots\right]^T \tag{12}$$

$$[N] = \begin{bmatrix} N_i & 0 & 0 & 0 & 0 & 0 & 0 & \bar{0}^D & \bar{0}^D & \bar{0}^D & \bar{0}^D & \bar{0}^D & \\ 0 & N_i & 0 & 0 & 0 & 0 & 0 & \bar{0}^D & \bar{0}^D & \bar{0}^D & \bar{0}^D & \bar{0}^D & \\ 0 & 0 & H_i & H_{xi} & H_{yi} & 0 & 0 & \bar{0}^D & \bar{0}^D & \bar{0}^D & \bar{0}^D & \bar{0}^D & \\ \ldots\ 0 & 0 & 0 & 0 & 0 & N_i & 0 & \bar{0}^D & \bar{0}^D & \bar{0}^D & \bar{0}^D & \bar{0}^D & \ldots \\ 0 & 0 & 0 & 0 & 0 & 0 & N_i & \bar{0}^D & \bar{0}^D & \bar{0}^D & \bar{0}^D & \bar{0}^D & \\ 0 & 0 & 0 & 0 & 0 & 0 & 0 & \bar{N}_i^D & \bar{0}^D & \bar{0}^D & \bar{0}^D & \bar{0}^D & \\ 0 & 0 & 0 & 0 & 0 & 0 & 0 & \bar{0}^D & \bar{N}_i^D & \bar{0}^D & \bar{0}^D & \bar{0}^D & \\ 0 & 0 & 0 & 0 & 0 & 0 & 0 & \bar{0}^D & \bar{0}^D & \bar{H}_i^D & \bar{H}_{xi}^D & \bar{H}_{yi}^D & \end{bmatrix}$$

In Eq. (12) D is the total number of delamination; $\bar{0}^D$ is a $1 \times D$ null row vector, and $\bar{N}_i^D$, $\bar{H}_i^D$, $\bar{H}_{xi}^D$, and $\bar{H}_{yi}^D$ are $1 \times D$ row vectors, which are defined as follows:

$$\bar{N}_i^D = [N_i \quad \cdots \quad N_i], \qquad \bar{H}_i^D = [H_i \quad \ldots \quad H_i]$$

$$\bar{H}_{xi}^D = [H_{xi} \quad \ldots \quad H_{xi}], \qquad \bar{H}_{yi}^D = [H_{yi} \quad \ldots \quad H_{yi}] \tag{13}$$

Based on the field assumptions and kinematic relations already described, the element displacement field $u(x, y, z, t)$ and the asso-

The preceding formulation results in 28 generalized nodal unknowns for a undelaminated plate element and $(28 + 5 \times D)$ generalized nodal unknowns for a delaminated element, where D represents the number of delamination present.

The equations of motion are obtained from the Hamilton's principle as follows:

$$\int_{t_0}^{t} \left[\int_V (\rho \ddot{u}_i \delta u_i + \sigma_{ij} \delta \varepsilon_{ij})\, \mathrm{d}V - \int_{\Gamma_\sigma} \bar{t}_i \delta u_i\, \mathrm{d}\Gamma \right] \mathrm{d}t = 0 \tag{16}$$

By substituting Eqs. (11) and (14) into Eq. (16), the finite element model of free vibration is obtained as follows:

$$([K] - \omega^2[M])\{d\} = 0 \tag{17}$$

where $[K]$ and $[M]$ are the stiffness and mass matrices, respectively. The quantity ω denotes the natural frequency, and $\{d\}$ represents the eigenvector of nodal displacements corresponding to an eigenvalue. The stiffness and mass matrices are defined as follows:

$$[K] = \int_V B_\varepsilon^T Q B_\varepsilon\, \mathrm{d}V, \qquad [M] = \int_V B_u^T Q B_u\, \mathrm{d}V \tag{18}$$

with the following definition of the operators:

$$B_u = L_u N, \qquad B_\varepsilon = L_\varepsilon N \tag{19}$$

IV. Results and Discussion

A number of case studies have been conducted to validate the developed procedure. Comparisons are made with analytical solutions, higher-order-theory-based results and experiments. Next, parametric studies are conducted to investigate the effects of number, placement, and size of delamination on the dynamic response of cross-ply composite plate.

To validate the model, first, the natural frequencies are computed and are compared with experimental results,[7] analytical solution,[7] and results from a higher-order theory.[13] Results are presented for

a $[0, 90]_{2s}$ carbon-epoxy cantilever composite beam plate with dimensions 12.7-cm (5-in.) length and 1.27-cm (0.5-in.) thickness as used in Ref. 7. The ply thickness is 0.0127 cm (0.005 in.). The material properties for the carbon-epoxy cantilever plate beam are $E_1 = 134.4$ GPa, $E_2 = 10.34$ GPa, $G_{12} = 5.0$ GPa, $\rho = 1477$ kg/m^3, and $\nu = 0.33$. A finite element mesh consisting of 30×5 four-noded plate elements is used to model both the present improved layerwise theory and the higher-order theory (HOT).[13] Table 1 presents the comparison of the fundamental natural frequencies between the undelaminated plate and delaminated plates with a single through-the-width, centrally placed delamination, of various size and location. In Table 1 the I0, I1, I2, and I3 indicate the ply level location of the delamination, measured from the midsurface. Thus I0 represents a delamination at the midsurface, and I1 represents the presence of delamination at the first interface measured from the midsurface, and a refers to the length of delamination. In terms of in-plane location, the midsection of the delamination coincides with the midsection of the plate. As seen from Table 1, results from the present theory agree very well with results obtained using experiments, analytical approach, and HOT. Figures 1a–1c present comparisons of the natural frequencies, obtained using the present theory and HOT, associated with the first and second bending modes and the first twisting mode for the same plate with a 40% delamination [of size 2 in. (5.08 cm)] located at various ply interfaces. The natural frequencies of the delaminated structure shift from the undelaminated one, more when the delamination is located near the midplane and less when the

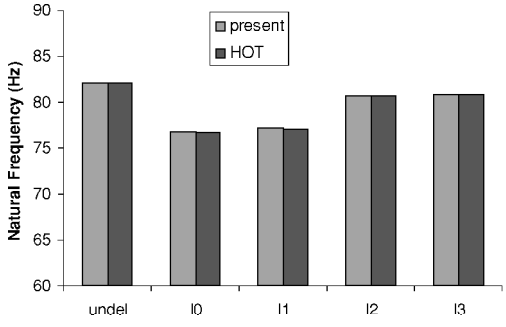

a) First bending mode

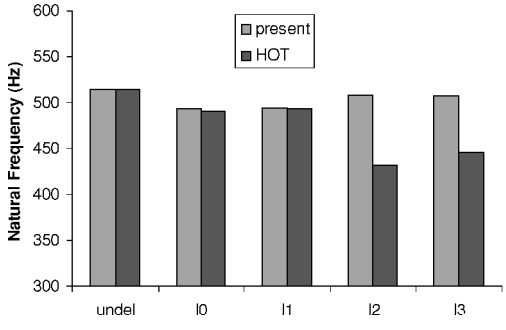

b) Second bending mode

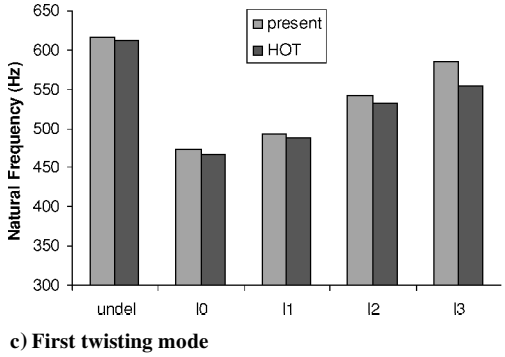

c) First twisting mode

Fig. 1 Natural frequencies of a cantilever plate ([0/90]2s) with a 2-in. (5.08-cm) delamination.

Table 1 Comparison of fundamental natural frequencies, single delamination of different size and ply level location

	I0				I1				I2				I3			
a, in.	Experiment[7]	Analytical model[7]	HOT[13]	Present	Experiment[7]	Analytical model[7]	HOT[13]	Present	Experiment[7]	Analytical model[7]	HOT[13]	Present	Experiment[7]	Analytical model[7]	HOT[13]	Present
0.0	79.83	82.042	82.11	82.133	79.83	82.042	82.11	82.133	79.83	82.042	82.11	82.133	79.83	82.042	82.11	82.133
1.0	78.17	80.133	81.37	81.431	77.79	81.385	81.42	81.485	80.12	81.461	81.92	81.960	75.96	81.598	81.94	81.974
2.0	75.38	75.285	76.73	76.812	75.13	78.103	77.11	77.187	79.75	79.932	80.65	80.741	68.92	80.383	80.83	80.882
3.0	66.96	66.936	67.57	67.641	67.96	71.159	68.42	68.498	76.96	76.712	77.44	77.787	62.50	77.698	78.04	78.226
4.0	57.54	57.239	56.89	56.940	48.37	62.121	58.04	58.113	72.46	71.663	71.66	73.116	55.63	73.147	73.21	73.967

delamination is located near the surface and away from the midplane. This trend is observed in the first three modes using the present analysis and in the first two modes using HOT. This discrepancy suggests that the ply level information from the present layerwise theory provides more accurate description of strain field, resulting in more accurate prediction of natural frequencies. Thus from Table 1 and Fig. 1, it can be concluded that the results obtained from the present analysis are highly comparable with the already published results from Refs. 7 and 13.

An experimental investigation is conducted next to further validate the developed theory. A set of carbon-cyanate $(0, 90)_{4s}$ laminated composite cantilever plate beams (as shown in Fig. 2) is manufactured using a hot press. The fiber used for the laminate is K1100 carbon, and the curing resin is 954-2A cyanate resin. The material properties for the laminated composite are as follows: $E_1 = 380$ GPa, $E_2 = 16.6$ GPa, $G_{12} = 4.2$ GPa, $\rho = 1800$ kg/m^3, $\nu_{12} = 0.31$, and $\nu_{23} = 0.42$. The dimensions of the cantilever plates are 31.1-cm length, 5.1-cm width, and 0.218-cm thickness. The ply thickness is measured to be 0.137 mm. The experimental setup using laser vibrometry testing is shown in Fig. 3a. The setup consists of the test specimen, mounted on a vice attached to a Newport RS4000 vibration isolation table, a scanning laser Doppler vibrometer (Polytec SLDV), a waveform generator (Agilient 33120A), and an ACX Quickpack power amplifier. The piezoelectric patch actuator, surface bonded approximately at a distance of 1.83 cm away from the fixed end, is used to excite the structure, while the laser scans the outer surface to measure transverse vibration and displacement. The size of the actuator is $5.1 \times 2.54 \times 0.051$ cm, and it consists of two stacked lead zirconate titanate (PZT) 5H wafers (Fig. 3b). The

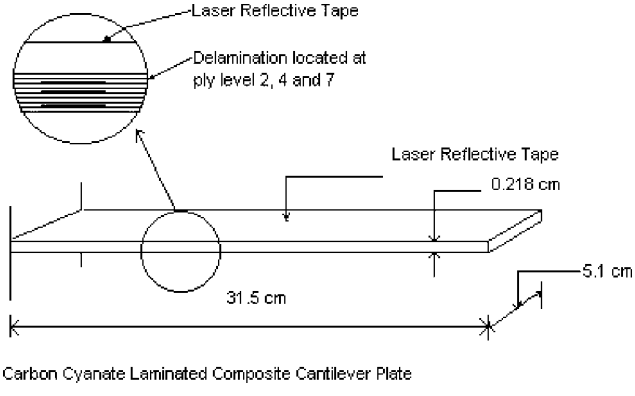

Fig. 2 Carbon-cyanate laminated composite cantilever plate with delamination.

Fig. 3a Experimental setup for laser vibrometry.

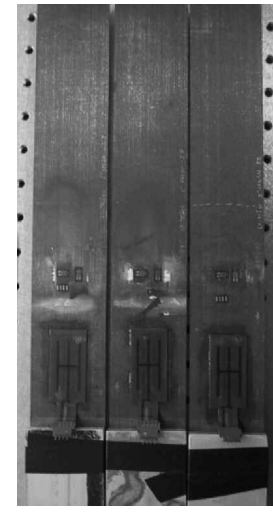

Fig. 3b Set of laminated composite cantilever plate with ACX PZT actuators (QP25N) attached near the fixed end.

material properties of the PZT (isotropic) are as follows: $E = 63$ GPa, $\rho = 7700$ kg/m^3, and $\nu = 0.28$ (Ref. 17). Four specimens, one undelaminated and the remaining three with embedded delamination at ply levels 2, 4, and 7, respectively, are used. One side of the plate is covered with a very thin, flexible laser-reflective tape to obtain better signal-to-noise ratio for the laser measurement. In all of the delaminated specimens, the delamination is seeded in the other half from the midplane, which is away from the laser-taped side. Thus the interfacial ply levels are numbered from the midplane and away from the reflective tape surface. The delamination is seeded using two very thin plastic release films placed between the interfaces of two laminae. In the first two specimens a delamination of size 5.1×5.1 cm (16% delamination) is seeded at a distance of 11 cm from the fixed end. In the experimental analysis the frequency response function (FRF) plots caused by the input excitation of periodic chirp or sine sweep are obtained for various frequency bandwidths. The FRF peaks denote the natural frequencies of the laminated composite specimen. Table 2 presents the comparison of first five natural frequencies, obtained experimentally, with the numerical results obtained using the developed theory and HOT. In the numerical analysis 30×5 four-noded elements are used to obtain the results using HOT,[13] and 30×4 elements are used to obtain the results using the present theory. The comparisons are presented for delamination located at three different ply levels, indicated by I2, I4, and I7. Table 2 shows that the numerical (present analysis and HOT) and the experimental results are within 8% of each other for the first five modes. The results obtained from the present theory are closer to the experimental results, further establishing the accuracy of the developed procedure. Also, the number of elements used in the present analysis is 20% fewer than those used in the HOT analysis to obtain similar levels of accuracy. The frequency shift caused by the presence of delamination is also clearly noticeable, becoming more pronounced at higher modes and when the delamination is embedded closer to the midplane of the composite laminate. Figures 4a–4d show the experimental vibration displacement shapes (VDS) at the fundamental flexural frequencies of the cantilever plate with no delamination and delamination of 5.1 cm at ply levels I7, I4, and I2. The effect of delamination is not clearly visible in the first bending mode.

The pronounced natural frequency shifts observed when the delamination is located closer to the midplane, as opposed to closer to the surface, with respect to the undelaminated structure can be empirically explained by computing the bending inertia. Assuming that the delamination causes sliding along the two delaminated surfaces, the bending inertia can be computed. For example, the inertia of undelaminated laminate Ih is $bh^3/12 = 0.083bh^3$, and the corresponding values for the delaminated laminate Id are $bh^3/12(14^3/16^3 + 2^3/16^3) = 0.056bh^3$ with delamination at the

Table 2 Comparisons of first five natural frequencies with ply level variation in delamination placement

Natural frequency	Undelaminated			I2			I4			I7		
	Experiment	HOT	Present	Experiment	HOT	Present	Experiment	HOT	Present	Experiment	HOT	Present
ω_1	41.26	42.08	40.152	40.00	41.89	40.046	40.31	41.96	40.088	40.94	42.06	40.132
ω_2	125.8	133.9	133.40	118.3	131.4	131.8	120.8	132.4	132.36	122.7	133.5	133.22
ω_3	255.1	260.2	250.44	249.4	258.4	249.5	250.6	258.9	249.81	250.6	259.5	249.61
ω_4	434.0	457.6	450.57	420.6	455.4	448.93	421.7	455.7	449.29	430.8	453.6	448.18
ω_5	703.8	717.4	686.19	628.6	678.4	664.27	639.5	692.0	671.21	690.6	695.8	678.03

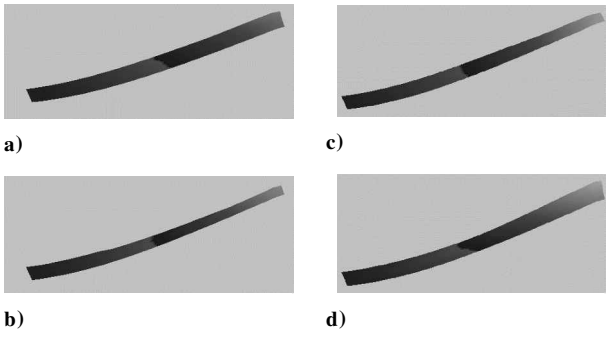

Fig. 4 VDS of the cantilever plate: a) undelaminated plate and b–d) single delamination at ply levels I7, I4, and I2, respectively.

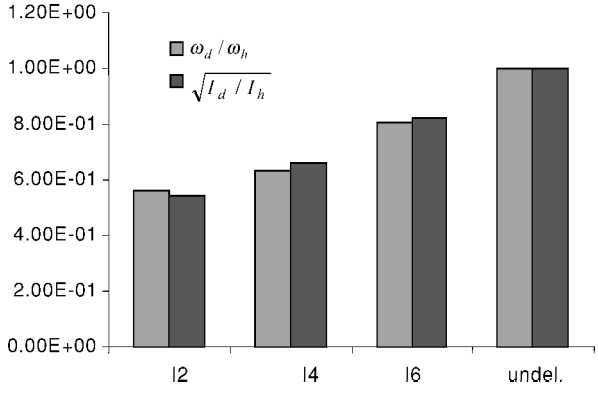

Fig. 5 Comparison of natural frequencies and bending inertia.

I6 ply level and $bh^3/12(1/2^3 + 1/2^3) = 0.0208bh^3$ with delamination at midsurface. Comparison of the inertias shows that the delamination near the surface reduces the second area moment of inertia by 33%, whereas delamination at the midsurface reduces the inertia by 75%. Thus, the natural frequency reductions of 25% when the delamination is at I6 interface level and 50% when the delamination is at midplane are meaningful because for a given Young's modulus natural frequencies are directly proportional to the square root of the bending inertia of the structure. A comparison of the reductions in natural frequencies and bending inertia, caused by delamination, is presented in Fig. 5. The figure shows comparable trends as the location of the delamination is shifted from midsurface toward the outer surface. This observation can be useful in damage characterization.

The results from the parametric study are presented next. The same plate, as used in the validation studies,[7] is used in this numerical investigation. First, the effect of through-the-thickness variation in delamination placement is investigated, and the results are compared with an undelaminated plate. Figures 6a–6c show the natural frequencies associated with the first and second bending modes and the first twisting mode for the composite plate with a 60% delamination (3 in.), of varying location (I0–I3), and the undelaminated plate. Similar trends in natural frequency shift, as noted during the validation studies, are observed. Figures 7a and 7b show the first bending and twisting mode shapes for the undelaminated plate, and the corresponding mode shapes of the delaminated plate with a 40% delamination located at midplane are shown in Figs. 7c and 7d. The

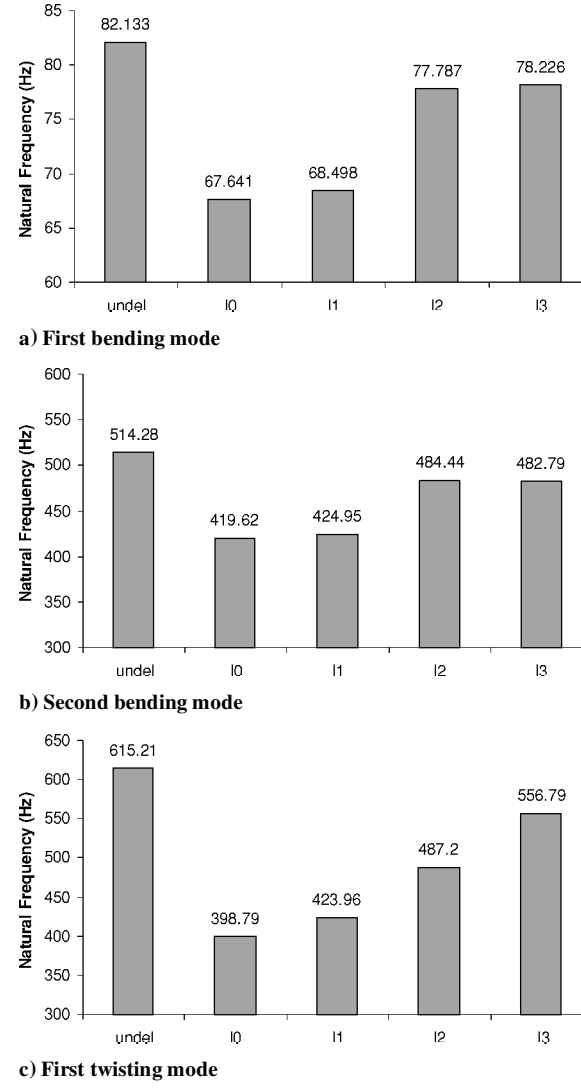

Fig. 6 Natural frequencies of a cantilever plate ([0/90]2s) with a 3-in. (7.62-cm) delamination.

effect of the delamination is significantly more observable in the first twisting mode of the delaminated plate than in the first flexural mode.

Next, numerical investigations are conducted to study the effects of in-plane variation in delamination placement and multiple delaminations of various sizes and placement. The geometry of the carbon-cyanate laminated composite cantilever plate with multiple delaminations is shown in Fig. 8. In this figure cases 1–4 represent variations in in-plane location of delamination, with respect to the fixed end. First, the effect of in-plane variation in delamination location is studied using a single delamination of size 6×5 cm (20% delamination) with varying locations along the in-plane (cases 1–3). As shown in Fig. 9, the effect is more pronounced in the natural frequency shift, from the undelaminated to the damaged structure, when the delamination is located near the fixed end. Once again, the delamination effect is more easily observable in the higher modes.

Next, numerical studies are conducted to investigate the effect of multiple delamination. Table 3 shows the first five natural frequencies for the composite plate (Fig. 8) with multiple delaminations located at different ply levels through the thickness direction. The in-plane location and size of the delamination is the same as in case 2 (Fig. 8). In Table 3, I( ) denotes the ply level location of the delamination, and notations I( ) + I( ) + ⋯ are used to describe multiple delamination cases with a single delamination of same size located at each ply level. It is observed (from Table 3) that increases in the number of equal size delamination affect the natural frequency shifts from the undelaminated structure. The frequency shifts are more significant when the multiple delaminations are located near the midplane, compared to the case where they are located closer to the free surface. The effects are also more pronounced at higher frequencies.

The effect of a combination of multiple delaminations located in the same ply level (I2 + I2 + I2) and distributed stepwise along different ply levels (I2 + I4 + I7 and I7 + I4 + I2; Fig. 8) is investigated next. Comparisons of the first five natural frequencies with the frequencies of the undelaminated plate, for all three cases, are presented in Table 4, and the percentage differences are shown in Fig. 10. It is observed that the frequency shifts caused by a combination of three delaminations located in the I2 plane are more pronounced than in the other cases. The second largest shifts are observed when the delamination located closest to the fixed end is also closest to the midplane (I2 + I4 + I7). Also, as seen from Fig. 10, the percentage shifts in natural frequencies are more pronounced at the higher modes.

Next, the effect of discrete multiple delaminations as opposed to a single delamination of the same total size, located in the same ply level, is investigated. Table 5 presents the first five natural frequencies of plates with two multiple, discrete delaminations of size 6 × 5 cm at the same ply level (I2), located 14 cm apart (D1) and

Table 3 Natural frequencies; multiple delamination at different ply levels

Hz	Undelaminated	I2 + I4	I2 + I7	I4 + I7	I2 + I4 + I7
ω_1	42.850	42.636	42.645	42.728	42.617
ω_2	135.54	133.01	133.26	134.07	132.90
ω_3	267.64	266.89	263.50	263.31	263.05
ω_4	465.57	459.25	453.29	454.19	451.86
ω_5	745.38	677.09	677.63	702.81	669.29

Table 4 Natural frequencies; multiple delamination at different in-plane locations

Hz	Undelaminated	I2 + I2 + I2	I2 + I4 + I7	I7 + I4 + I2
ω_1	42.850	42.43	42.499	42.648
ω_2	135.54	128.87	129.66	133.14
ω_3	267.64	250.63	252.69	260.73
ω_4	465.57	428.67	436.28	447.18
ω_5	745.38	630.12	654.55	664.68

Table 5 Natural frequencies; multiple discrete and single continuous delamination

Hz	Undelaminated	D1	D2	D3
ω_1	42.850	42.591	42.433	40.756
ω_2	135.54	130.70	128.58	113.03
ω_3	267.64	250.80	251.29	209.78
ω_4	465.57	432.97	439.13	400.07
ω_5	745.38	669.62	661.58	650.52

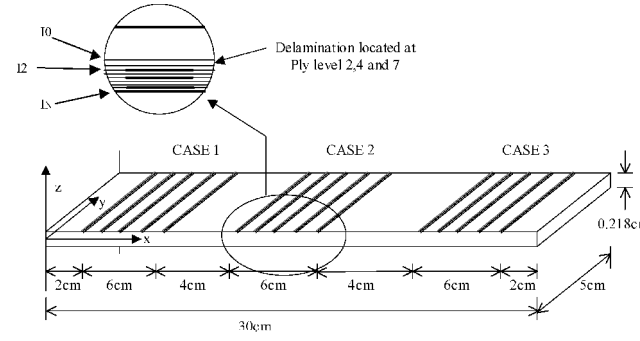

Fig. 8 Composite plate with multiple delamination.

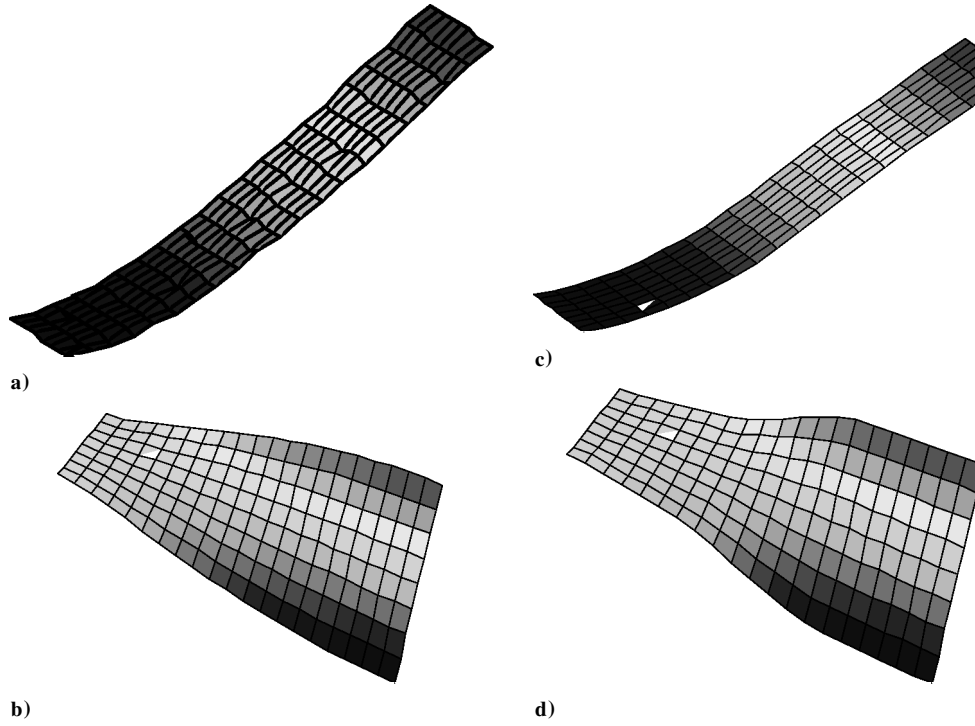

Fig. 7 Mode shapes of the $[0/90]_{2s}$ cantilever plate: a) and b) first bending and twisting modes with undelaminated plate and c) and d) first bending and twisting modes with plate having 2-in. (5.08-cm) delamination.

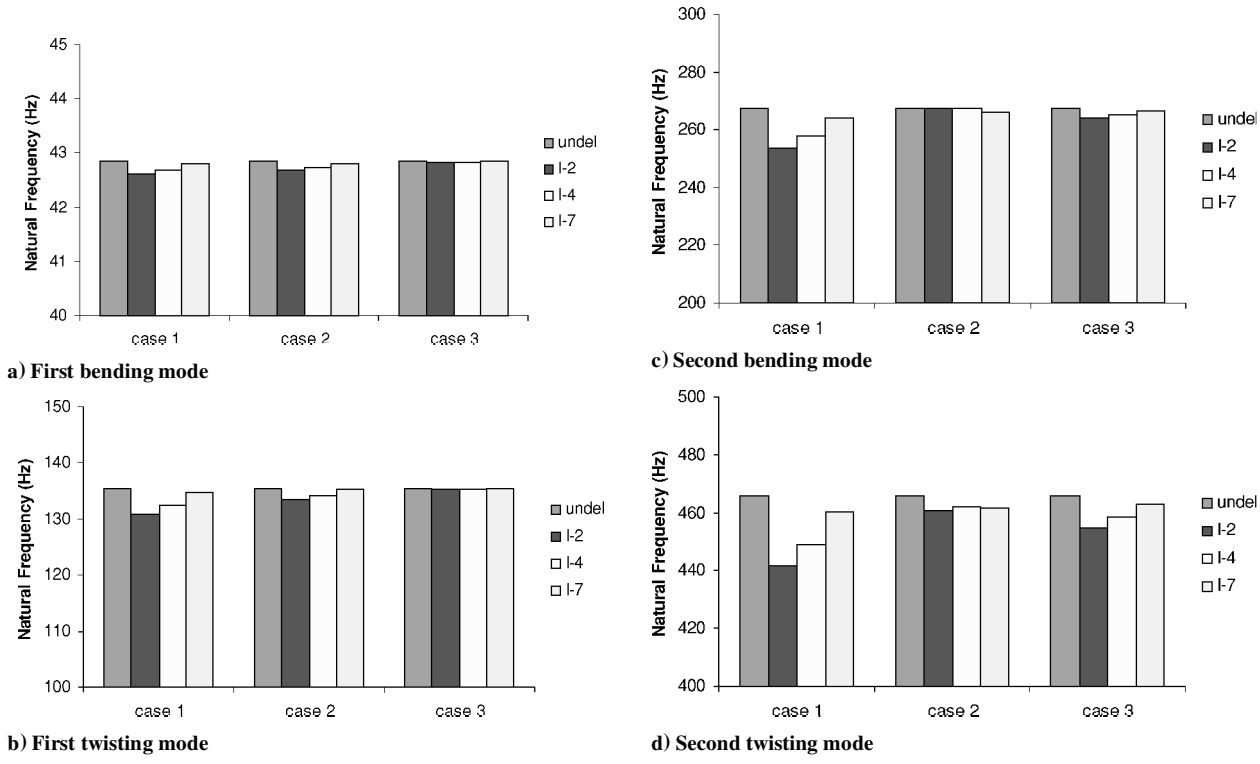

Fig. 9 Change in natural frequencies with in-plane variations of a single delamination.

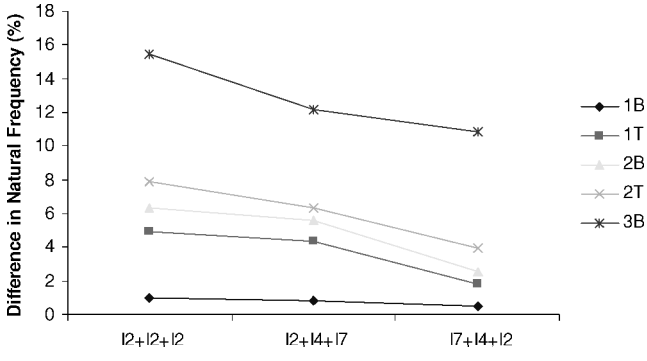

Fig. 10 Difference in natural frequencies with in-plane variations of multiple delaminations (B, bending; T, twisting).

1 cm apart (D2), and a plate with a single continuous delamination of size 13 × 5 cm (D3). In all of these cases (D1, D2, and D3), the delamination initiates at a distance of 2 cm from the fixed end. It is observed that frequency shifts caused by the presence of delamination is significantly more pronounced for the case with single delamination compared to the cases with multiple discrete delaminations. This indicates that a continuous delamination affects the global stiffness more significantly than a number of discrete ones of comparable length. The shifts in natural frequencies are more pronounced when the discrete delaminations are further apart (D1), compared to the case where they are closely spaced (D2). This is because in the latter case both the delaminations are located closer to the fixed end where maximum strains develop.

V. Conclusions

An investigation on the dynamic response of cross-ply composite plates, with embedded multiple delamination, was conducted. An improved layerwise laminate theory was used to model the displacement fields, and Heaviside step functions were used to represent the separation and slipping caused by delamination. The results from the present theory were validated with available experimental and numerical results. Experiments were also conducted for further validation. Parametric studies were conducted to investigate the effects of number, placement, and size of delamination on the dynamic response. The following important observations were made from the present study:

1) The results from the present theory correlate very well with those obtained using a higher-order theory and available experiments.

2) The present results also correlate very well with the results from the experiments conducted.

3) Changes in natural frequency between undelaminated and damaged cantilever composite plate are observed. The changes are more pronounced when the delamination or a combination of multiple delaminations are located closer to the midplane and closer to the fixed end.

4) The global effect of a single long delamination is more significant than that caused by discrete multiple delaminations.

Acknowledgments

The research is supported by NASA Langley Research Center, Hampton, Virginia, Grant NAG-1-2283, Technical Monitor D. Ambur.

References

[1]Barbero, E. J., and Reddy, J. N., "Modeling of Delamination in Composite Laminates Using a Layer-wise Plate Theory," *International Journal of Solids and Structures*, Vol. 28, No. 3, 1991, pp. 373–388.

[2]Chattopadhyay, A., and Gu, H., "A New Higher-Order Plate Theory in Modeling Delamination Buckling of Composite Laminates," *AIAA Journal*, Vol. 32, No. 8, 1994, pp. 1709–1718.

[3]Chattopadhyay, A., and Gu, H., "Delamination Buckling and Postbuckling of Composite Cylindrical Shells," *AIAA Journal*, Vol. 34, No. 6, 1996, pp. 1279–1286.

[4]Chattopadhyay, A., and Gu, H., "Elasticity Based Solutions for Buckling of Composite Plates," *AIAA Journal*, Vol. 36, No. 8, 1998, pp. 1529–1534.

[5]Gu, H., and Chattopadhyay, A., "An Experimental Investigation of Delamination Buckling and Postbuckling of Composite Laminates," *Composite Science and Technology*, Vol. 59, 1999, pp. 903–910.

[6]Zhou, X., and Chattopadhyay, A., "Modeling of Laminated Shell Structures Addressing Transverse Stress and Interlaminar Continuity," *Proceedings of the 42nd AIAA/ASME/ASCE/AHS/ASC Structures, Structural Dynamics, and Materials Conference and Exhibition* [CD-ROM], AIAA, Reston, VA, 2001.

[7]Shen, M. H., and Grady, J. E., "Free Vibrations of Delaminated Beams," *AIAA Journal*, Vol. 30, No. 5, 1992, pp. 1361–1370.

[8]Crawley, P., and Adams, R. D., "A Vibration Technique for Nondestructive Testing of Fiber Composite Structures," *Journal of Composite Materials*, Vol. 13, No. 2, 1980, pp. 161–175.

[9]Williams, E. J., Messina, A., and Payne, B. S., "A Frequency-Change Correlation Approach to Damage Detection," *Proceedings of the 15th International Modal Analysis Conference*, Vol. 1, Society of Experimental Mechanics, Bethel, CT, 1997, pp. 652–657.

[10]Luo, H., and Hanagud, S., "Delamination Modes in Composite Plates," *Journal of Aerospace Engineering*, Vol. 9, No. 4, 1996, pp. 106–113.

[11]Lestari, W., and Hanagud, S., "Health Monitoring of Structures: Multiple Delamination Dynamics in Composite," *Proceedings of the 40th AIAA/ASME/ASCE/AHS/ASC Structures, Structural Dynamics, and Materials Conference and Exhibition* [CD-ROM], AIAA, Reston, VA, 1999.

[12]Thornburgh, R., and Chattopadhyay, A., "Modeling the Behavior of Laminated Composites with Delamination and Matrix Cracks," *AIAA Journal*, Vol. 39, 2001, pp. 153–160.

[13]Thornburgh, R., and Chattopadhyay, A., "Modeling the Dynamic Effects of Delamination in Adaptive Composite Laminate," AIAA Paper 2002-1443, April 2002.

[14]Cho, M., and Kim, J. S., "Higher-Order Zig-Zag Theory for Laminated Composites with Multiple Delaminations," *Journal of Applied Mechanics*, Vol. 68, Nov. 2001, pp. 869–877.

[15]Kim, J. S., and Cho, M., "Buckling Analysis for Delaminated Composites Using Plate Bending Elements Based on Higher-Order Zig-Zag Theory," *International Journal for Numerical Methods in Engineering*, Vol. 55, No. 11, 2002, pp. 1323–1343.

[16]Kim, H. S., Zhou, X., and Chattopadhyay, A., "Interlaminar Stress Analysis of Shell Structures with Piezoelectric Patch Including Thermal Loading," *AIAA Journal*, Vol. 40, No. 12, 2002, pp. 2517–2525.

[17]*Cymer ACX Quickpack Actuators Manual*, Active Control eXperts, Inc., Cambridge, MA, 2001.

A. N. Palazotto
Associate Editor